NACA

RESEARCH MEMORANDUM

AERODYNAMIC CHARACTERISTICS OF NACA RM-10 MISSILE IN 8- BY 6-FOOT SUPERSONIC WIND TUNNEL AT MACH NUMBERS FROM 1.49 TO 1.98

III - ANALYSIS OF FORCE DISTRIBUTION AT ANGLE OF ATTACK (STABILIZING FINS REMOVED)

By Roger W. Luidens and Paul C. Simon

Lewis Flight Propulsion Laboratory
Cleveland, Ohio

NATIONAL ADVISORY COMMITTEE
FOR AERONAUTICS

WASHINGTON
December 12, 1950

Classification cancelled (or changed to Unclassified)

By authority of: NASA Tech Pub Announcement
(OFFICER AUTHORIZED TO CHANGE)
91 21 Oct 65

By .....

.....
GRADE OF OFFICER MAKING CHANGE)

21 Apr 62
DATE

NATIONAL ADVISORY COMMITTEE FOR AERONAUTICS

AERODYNAMIC CHARACTERISTICS OF NACA RM-10 MISSILE IN 8- BY 6-FOOT SUPERSONIC WIND TUNNEL AT MACH NUMBERS FROM 1.49 TO 1.98

III - ANALYSIS OF FORCE DISTRIBUTION AT ANGLE OF ATTACK (STABILIZING FINS REMOVED)

By Roger W. Luidens and Paul C. Simon

SUMMARY

An analysis of the force distribution on a slender pointed body of revolution at angle of attack was made utilizing pressure-distribution data and balance measurements. The data were obtained in the NACA Lewis 8- by 6-foot supersonic tunnel at Mach numbers of 1.49, 1.59, 1.78, and 1.98 and for a range of angles of attack from 0° to 9°. The Reynolds number based on the model length was approximately 30,000,000. The parabolic body investigated was the half-scale model of the NACA supersonic flight-research missile designated RM-10 (with stabilizing fins removed). A second model consisting of a cone-cylinder combination was investigated to isolate the effect of profile curvature.

The inability to predict the normal force distribution due to angle of attack on slender bodies of revolution by the existing linearized potential theory was due in part to inaccurate prediction by the theory of the pressure distribution due to angle of attack on bodies with curved profiles, and in part to neglecting the effects of cross-flow separation by the theory. A concept of the linearized potential theory (in which the radius of the body is assumed to approach zero) is presented, which approximately eliminates the shortcomings of the theory with regard to the curved profiles.

The axial friction and fore pressure force remained essentially constant with angle of attack. The increase in total axial force with angle of attack was primarily due to an increase in base pressure force.

INTRODUCTION

Many methods are available for predicting the aerodynamic forces acting on slender bodies of revolution (at angle of attack) moving at supersonic speeds. Two representative methods for predicting the normal forces on slender bodies of revolution inclined to a supersonic stream are linearized potential theory, which seriously underestimates the measured values, and the method of reference 1, which greatly improves the estimation by modifying the potential theory in an attempt to account for viscous effects. The assumption of constant separation made in reference 1, however, is inconsistent with the pressure distributions observed on the RM-10 model (reference 2). In addition, deviations of experimental pressure distribution from potential theory exist over many regions of the body not appreciably influenced by viscous effects.

An investigation was therefore conducted to determine the theoretical and experimental distributions of the normal and axial forces and to study the origin of the discrepancies that occur between theory and experiment. Use was made of the RM-10 data presented in references 2 and 3 and the pressure-distribution data obtained with a second model. The investigation covers a range of Mach numbers from 1.49 to 2.00, angles of attack from 0° to 9°, and a test Reynolds number of approximately 30,000,000 based on the length of the RM-10 model.

APPARATUS AND PROCEDURE

Data from the RM-10 (fig. 1(a)) investigation of references 2 and 3 are presented herein. A second model (fig. 1(b)) having a length of 55 inches, a maximum diameter of 2.5 inches, and a fineness ratio l/D of 21.9 has also been investigated. The body consisted of a 12° vertex angle cone (nose was blunted by removing 1/8 inch from the tip) extending 3.20 diameters, and a cylindrical section 15.4 body diameters long joined by a curved section faired between the cone and the cylinder. Static-pressure orifices were located in a longitudinal row on the model surface at every inch from station 2 inches to 17 inches and every 2 inches from station 17 inches to 49 inches. The support system described in reference 2 was used for the cone-cylinder model.

Experimental pressure data were obtained for nominal free-stream Mach numbers of 1.5, 1.6, 1.8, and 2.0, for orifice radial positions of $\theta = 0°$ and 180°, and for angles of attack of 0° and 8°. The Reynolds number based on the model length was approximately 23,000,000.

SYMBOLS

The following symbols are used in this report:

C	coefficient
C_p	pressure coefficient, $\frac{p-p_0}{q_0}$
c	a constant
$c_{d,c}$	section drag coefficient of a circular cylinder per unit length in terms of its diameter
D	maximum body diameter
f	local friction force
k	a constant
M	Mach number
p	static pressure
q	$\frac{\gamma}{2} pM^2$
R_x	Reynolds number, $\rho Ux/\mu$
S	maximum cross-sectional area
S_b	model base area
S_G	model plan-form area
U	velocity
v_r	radial velocity component (cylindrical coordinates)
v_x	axial velocity component
v_θ	tangential velocity component (cylindrical coordinates)
x,b	coordinates of model
x,r,θ	cylindrical coordinates ($\theta = 0$ in plane of angle of attack and to windward)

α	angle of attack
β	cotangent of Mach angle, $\sqrt{M^2-1}$
γ	ratio of specific heats, 1.40
Δ	conditions for model due to angle of attack
δ	boundary-layer thickness
δ^*	boundary-layer displacement thickness
η	ratio of drag coefficient for circular cylinder of finite length to that for cylinder of infinite length
μ	viscosity
ρ	density

Subscripts:

0	free-stream conditions
2	conditions for model due to angle of attack
A	axial force (positive to rearward)
a	station axial force
b	base of model
f	due to friction
L	leeward side or surface of model
l	length of model
N	normal force (positive to leeward)
n	station normal force
p	pressure
W	windward side or surface of model

METHOD OF COMPUTATION AND REDUCTION OF DATA

The experimental pressure distribution and the force measurements for the RM-10 model, which are presented in references 2 and 3, were reduced to normal and axial force coefficients. The incremental normal and axial pressure force coefficients (due to angle of attack) were obtained by graphically integrating the experimental incremental pressure coefficients $C_{p,2}$. Force coefficients are presented in terms of the model maximum cross-sectional area S with the exception of the station force coefficients, which are based on the individual station diameters.

Axial force data as a function of Mach number for angles of attack of 4° and 9° were obtained from cross plots because the experimental values recorded for the pressure model and the balance model were obtained at slightly different angles of attack.

The theoretical incremental pressure coefficient associated with angle of attack for the linearized potential theory was given in references 2 and 3 as

$$C_{p,2} = 4\alpha \cos\theta \frac{db}{dx} + \alpha^2(1 - 4\sin^2\theta) \tag{1}$$

Appropriate integrations (reference 3) of equations (1) over the body surface yield the following normal and axial force coefficients:

$$\Delta C_{n,W} = \pi\alpha \frac{db}{dx} - \frac{\alpha^2}{3} \tag{2}$$

$$\Delta C_{n,L} = \pi\alpha \frac{db}{dx} + \frac{\alpha^2}{3} \tag{3}$$

$$\Delta C_a = -\pi\alpha^2 \frac{db}{dx} \tag{4}$$

$$C_N = 2\alpha \frac{S_b}{S} \tag{5}$$

$$\Delta C_A = -\alpha^2 \frac{S_b}{S} \tag{6}$$

The normal force coefficient was also computed by the formula given in reference 1:

$$C_N = 2\alpha\left(\frac{S_b}{S}\right) + \eta c_{d,c}\alpha^2\left(\frac{S_G}{S}\right) \qquad (7)$$

Based on the conditions of this investigation and the criterions of reference 1, the value of η was taken as 0.71 and $c_{d,c}$ as 1.2.

RESULTS AND DISCUSSION

The aerodynamic forces acting on a body moving in a viscous fluid consist of the pressure forces associated with the acceleration of the fluid about the body and the shear forces resulting from the viscous attachment of the fluid to the body. For configurations with axial symmetry, these forces on the body are conveniently analyzed in terms of components directed normal and parallel to the body axis.

Normal Forces

A comparison of the measured total normal force coefficient and the values obtained by integration of the experimental pressure distribution coefficient with angle of attack for a range of Mach numbers is presented in figure 2. The difference between the total normal force and the normal pressure force is the contribution of the friction, which is shown to be negligible. The conclusion that the normal pressure force represents the total normal force acting on the body is substantiated in part by the data from two-dimensional cylinders normal to a subsonic stream, which show that the measured total drag force agrees closely with the drag force calculated from the pressure distribution (for example, reference 4). Additional verification is presented in appendix A by an analytical analysis of the shear forces. The results of the analysis are included in figure 2 as zone A, which also evidences that the friction normal force is very small within the angle of attack range where the measured normal force is appreciable. (A small friction force does not preclude an effect of viscosity on the pressure distribution; in fact this effect may be appreciable, as indicated in reference 1.)

Compared with the experimentally observed variation of normal force coefficients C_N with angle of attack α in figure 2 are the potential flow theory (equation (5)) and a modification of this theory given in appendix A, which accounts for the boundary-layer displacement thickness observed at zero angle of attack. The increase in the normal force coefficient due to the boundary-layer displacement thickness is represented by zone B. Both theories yield a linear variation of C_N with α and do not approximate the experimental results, which lie considerably above these theories and show an increasing normal force curve slope with increasing angle of attack.

The method of reference 1 (equation (7)), which assumes a viscous separation of the cross-flow along the length of the model, shows very close agreement with the data. The significance of this agreement, however, remains to be determined. None of the theories predict the increased normal force observed with increasing free-stream Mach number.

In order to facilitate further analysis of the normal pressure force distribution on the body, the experimental station normal forces were separated into windward and leeward coefficients ($\Delta C_{n,W}$ and $\Delta C_{n,L}$, the sum of which is the total station coefficient). The variation of these coefficients with angle of attack for six representative longitudinal model stations is presented in figure 3. For comparison, the local normal force coefficients calculated by potential theory (equations (2) and (3)) are also presented.

The potential theory best predicts the station normal force coefficient for both windward and leeward sides at the forward stations. At the mid and aft stations the leeward normal force coefficients are greater than predicted by potential theory. This effect may not be arbitrarily charged to separation of the cross flow, as might be implied from the agreement shown in figure 2 between the method of reference 1 and the total force. The normal force coefficient, observed at the mid-section of the windward side of the body, which is not subject to separation, is also greater than that predicted by theory. The pronounced deviation of the experimental results from the theory on the aft-lee side of the body (stations 58 and 70) is primarily associated with cross-flow separation. The agreement on the windward side in this region, however, is not adversely effected by the separation on the lee side. Thus, the possible argument that the cross-flow separation of the leeward surface fore and mid-sections of the model may appreciably affect the normal force over the fore and mid-sections of the windward surface is ruled out.

The excess lift, above that predicted by the theory, observed over both the lee and windward sides of the body mid-section results from an antisymmetrical-type pressure distribution that contributes appreciably to the total body lift. The excess of lift observed ahead of station 45 inches is slightly less on the leeward than on the windward side, and it is noted that the effect of boundary-layer accretion (without the formation of vorticity) on the forward-lee side of the body (reference 2) is to decrease the lift on the lee side of the body. An insight into a possible origin of the pressure distribution that gives rise to the excess of lift observed over the mid-sections of the body may be found in the equation for the pressure distribution due to angle of attack (equation (1)), which contains a term that is antisymmetrical about the body $\left(4\alpha \cos \theta \frac{db}{dx}\right)$ and results from the doublet distribution assumed on the body axis. The antisymmetrical term alone yields the normal force at a station. Thus it is logical to presume that the increased normal force, over that predicted by equation (1), observed on both the windward and leeward sides of the body mid-section arises for the most part from a shortcoming of the potential theory. The inability of the existing potential theory to predict the normal force coefficient therefore arises from (1) the failure of the existing theory to accurately predict the potential flow pressure distribution and (2) the neglect of viscous effects which result in cross-flow separation over some regions of the body.

In an attempt to determine how the discrepancies between the experimental results and the potential theory which are not chargeable to viscous effects are affected by model contour, a pressure-distribution investigation was conducted on a second model (fig. 1(b)) composed of a cone gradually faired into a cylinder. The incremental longitudinal pressure coefficient distribution for the windward side, $\theta = 0^\circ$ and the leeward side, $\theta = 180^\circ$ (the radial positions most significant with respect to the pressure influence on the normal force) are presented in figure 4 for $\alpha = 8^\circ$ at approximately the same Mach numbers as the RM-10 data.

The experimentally observed results show the best agreement with the potential theory on the windward side of the body for the regions where the body profile has constant slope (that is, the conical and cylindrical sections). On the lee side, close agreement was obtained over the cone but not over the cylinder, presumably because of cross-flow separation. Over the curved section of the model, the experimental pressures at all Mach numbers are greater on the windward and less on the leeward side of the model than those predicted by linearized theory. The same type of deviation from

theory was observed in the RM-10 data reproduced in figure 5. Profile curvature therefore has an effect on the pressure distribution that is not wholly accounted for by linearized potential theory. Appendix B presents a discussion of an assumption in the theory that results in this type of discrepancy and suggests a concept (which is not rigorous) that approximately corrects the shortcoming.

Axial Force

The axial force is the sum of the fore pressure force, the base pressure force, and the friction force. The distribution of the incremental station axial fore pressure force coefficient (due to angle of attack) $\Delta C_{a,p}$ for several representative stations is shown in figure 6 as a function of angle of attack. Except for stations 6 and 18, the potential theory (equation (4)) accurately predicts the station axial fore pressure force on the body despite the presence of cross-flow separation and some shortcomings of the existing linearized potential theory, which have an adverse effect on the prediction of normal force.

The increment of axial fore pressure force coefficient $\Delta C_{A,p}$ for the Mach numbers investigated is presented in figure 7 as a function of angle of attack. Also presented is the potential theory prediction of the axial force (equation (6)), which yields a thrust force proportional to the square of the angle of attack. The experimentally observed increment of axial fore pressure force coefficient is in general in the thrust direction, but is of much smaller magnitude than that predicted by theory. The high experimental axial fore pressure force as well as the experimental increase with increasing free-stream Mach number is associated with the flow about the forward portion of the body (fig. 6). It is emphasized that the maximum change in the incremental axial fore pressure force coefficient shown in figure 7 represents a variation of 4 percent or less in the total axial force. This magnitude is evident in figure 8, which shows the total axial force coefficient C_A and its component parts. Relative to the total axial force coefficient, the axial fore pressure force coefficient $C_{A,p}$ decreases only slightly with angle of attack and is very nearly equal to the value predicted by linearized theory for $\alpha = 0$ (reference 3). Most of the increase in total axial force with angle of attack is accounted for by the increase in base force shown in figure 8(c).

The axial friction force was calculated by subtracting the axial fore and base pressure forces from the total axial force. Figure 8(d) shows that within the accuracy of the experiment the axial friction force coefficient $C_{A,f}$ remains relatively constant with angle of attack, a result not readily anticipated in light of the pronounced circumferential variation in the boundary layer with angle of attack reported in reference 2.

1423

SUMMARY OF RESULTS

An analysis of the force distribution over a slender pointed nose body of revolution at angles of attack between 0° and 9° was made from data obtained in an investigation conducted in the NACA Lewis 8- by 6-foot supersonic wind tunnel at free-stream Mach numbers of 1.49, 1.59, 1.78, and 1.98 at a Reynolds number of approximately 30,000,000. The following results were obtained:

1. The contribution of the skin friction to the total normal force observed on the body at angle of attack was negligible, and the normal pressure force represents the total force acting normal to the body axis.

2. The existing linearized potential theory underestimates the normal force on the RM-10 for two reasons: (1) The theory does not accurately predict the potential flow pressure distribution due to angle of attack on bodies of revolution having curved profiles. (2) Separation of the cross flow exists over some regions of the body.

3. The axial friction force and axial fore pressure force remained essentially constant with angle of attack.

4. The increase in total axial force with angle of attack was primarily due to an increase in base pressure force.

Lewis Flight Propulsion Laboratory,
National Advisory Committee for Aeronautics,
Cleveland, Ohio.

APPENDIX A

BODY NORMAL FORCES AS AFFECTED BY FLUID VISCOSITY

Viscous forces in a fluid may affect the normal force on a body of revolution inclined to a supersonic stream in several ways: (1) by shear forces acting on the body; (2) by changes in pressure on the body as a result of boundary-layer displacement thickness; and (3) by changes in pressure on the body due to flow separation. In this appendix the magnitude of the first two effects is examined.

Fluid shear effect. - The contribution of the fluid shear force to the normal force depends on the local skin-friction coefficient and local inclination of the flow with respect to the body axis. The local friction force is

$$df = C_f q_0 b \, d\theta \, dx \tag{8}$$

The local inclination of the stream given in reference 2 is represented by

$$\frac{v_\theta}{U_0} = 2\alpha \sin \theta \tag{9}$$

and

$$\frac{v_r}{U_0} = \frac{db}{dx}$$

The station normal force may then be expressed as

$$n_f = 2q_0 b \left(2\alpha \int_0^\pi C_f \sin^2 \theta \, d\theta - \frac{db}{dx} \int_0^\pi C_f \cos \theta \, d\theta \right) \tag{10}$$

Assuming that C_f may be replaced by the constant mean value of 0.0021 (based on wetted area) found experimentally to exist at $M_0 = 1.98$ and $\alpha = 0$, the station normal force coefficient per radian due to friction becomes

$$\frac{C_{n,f}}{\alpha} = \frac{n_f}{2q_0 b\alpha} = C_f\pi = 0.0066 \qquad (11)$$

Integrating the station normal force over the length of the body yields, for the normal force coefficient due to friction on the RM-10, $C_{N,f}/\alpha = 0.0764$ (based on maximum cross-sectional area) compared with $C_N/\alpha = 0.734$ from potential theory, or approximately 10 percent of the potential theory and 3 percent of the measured total normal force coefficient at $\alpha = 8.61^\circ$, where the measured value is appreciable (fig. 2). It was found experimentally that the axial friction force remains constant with angle of attack, although the distribution of local friction undoubtedly changes. Such changes in local friction about the body affect the normal friction force through the first term in equation (10), but not appreciably. It may therefore be concluded that for the RM-10 the friction normal force is small.

Boundary-layer displacement thickness effect. - The equation for the normal force coefficient is

$$C_N = \frac{1}{S}\int_0^l \int_0^{2\pi} C_{p,2} \cos\theta b \, d\theta dx \qquad (12)$$

Utilizing linearized potential theory and including the boundary-layer displacement thickness in the manner of reference 6, the equation for the pressure coefficient due to angle of attack (equation (1)) becomes

$$C_{p,2} = 4\alpha \cos\theta \left(\frac{db}{dx} + \frac{d\delta^*}{dx}\right) + \alpha^2(1 - 4\sin^2\theta) \qquad (13)$$

This method assumes the boundary layer remains symmetrically disposed about the body at angle of attack. For turbulent boundary layer of the form consistent with the profile observed on the RM-10, reference 2 gives for the boundary-layer thickness

$$\delta = kxR_x^{-1/5} \qquad (14)$$

and

$$\frac{d\delta^*}{dx} = \frac{4}{5}\left(\frac{\delta^*}{\delta}\right) kR_x^{-1/5} \qquad (15)$$

Substituting in equation (13) and integrating in accordance with equation (12) over the RM-10 where $\delta = 1.0$ inch, as observed in the plane of the base at $M_0 = 1.98$, $k = 0.423$ and $\frac{\delta^*}{\delta} = 0.235$ (reference 7), the normal force coefficient per radian due to the boundary-layer displacement thickness is $C_{N,\delta^*}/\alpha = 0.216$ as compared with the potential value of $C_N/\alpha = 0.734$. The contribution of the boundary layer to the normal force amounts to approximately 30 percent of the potential theory and 9 percent of the measured total normal force coefficient at $\alpha = 8.61^\circ$.

The assumption that the boundary layer remains symmetrically disposed about the body at angle of attack is inconsistent with the experimentally observed results of reference 2, which showed a marked shift of the boundary layer from the windward to the leeward side of the model. The present calculation, however, is useful to show an order of magnitude of the effect.

APPENDIX B

EFFECT OF BODY PROFILE CURVATURE ON POTENTIAL FLOW PRESSURE DISTRIBUTION DUE TO ANGLE OF ATTACK

Part of the discrepancy between the experimentally observed and theoretically predicted pressures on the bodies investigated has been determined to be associated with the curvature of the profiles. It is now desirable to review the existing theory to determine what approximations in the theory may have led to this shortcoming and how the theory may be modified to account for this effect. A comparison of the theoretical results, developed in references 2 and 5, for determining the flow about a body inclined to a supersonic stream reveals that the assumption of either subsonic or supersonic flow yields the same solutions. Because the development of the subsonic equations (reference 5) presents an easier physical picture of the quantities involved, this concept will be used.

The equation for the perturbation velocity due to angle of attack is (reference 2)

$$\frac{v_{x,2}}{U_0} = -2\alpha \cos\theta \left(\frac{db}{dx}\right)$$

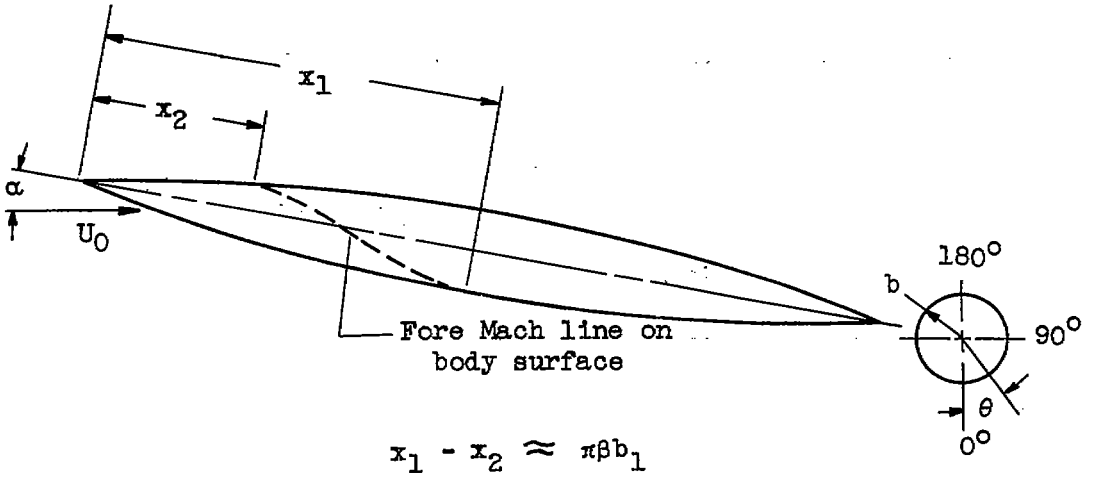

$$x_1 - x_2 \approx \pi\beta b_1$$

The implication in the subsonic case is that the component of flow normal to the body axis at any point on the body surface x_1 of the preceding sketch is influenced by the body slope in the plane perpendicular to the body axis at x_1. In the supersonic case, however, point $(x_1, b_1, \theta = 0)$ is influenced only by that portion of the body along and ahead of the fore Mach cone of the point under consideration. Because for the subsonic case the effect of angle of attack according to the theory arises only from the local body slope in a plane normal to the axis through the point of interest, it is presumed that in the supersonic case the effect of angle of attack arises only along the fore Mach line from the point under consideration. For bodies developed from profiles with curvature, the fore Mach line traverses regions of varying slope (db/dx) between x_1 and x_2. The influence of the slope at various positions on the fore Mach line has not been determined; however, the use of an average value such as the slope at $x_1 - \frac{\pi}{2}\beta b_1$ was used in this analysis. Other theoretical or physical averages could possibly be employed to advantage. It is of interest that such a concept does not influence the existing solutions in a cylinder or cone. The theoretical results yielded by this concept (which is not rigorous) are compared with the experimentally observed results in figures 9 to 11 and show an improved agreement with experimental results except where cross-flow separation is known to exist.

The distribution of incremental pressure coefficient as calculated by the stepwise doublet distribution method of reference 8, and defining $C_{p,2} = \alpha^2 - 2\frac{v_{x,2}}{U_0}$, is presented in figure 9 for the RM-10 model when $\theta = 0^\circ$ and 180°, $M_0 = 1.98$, and $\alpha = 8.61^\circ$. This solution shows that in general the prediction of the magnitude and trends of the pressures is improved. The normal force coefficient obtained by the integration of this pressure distribution is presented in figure 11 and shows only a small improvement over the normal force determined by equation (5).

REFERENCES

1. Allen, H. Julian: Estimation of the Forces and Moment Acting on Inclined Bodies of Revolution at High Fineness Ratio. NACA RM A9I26, 1949.

2. Luidens, Roger W., and Simon, Paul C.: Aerodynamic Characteristics of NACA RM-10 Missile in 8- by 6-Foot Supersonic Wind Tunnel at Mach Numbers from 1.49 to 1.98. I - Presentation and Analysis of Pressure Measurements (Stabilizing Fins Removed). NACA RM E50D10, 1950.

3. Esenwein, Fred T., Obery, Leonard J., and Schueller, Carl F.: Aerodynamic Characteristics of NACA RM-10 Missile in 8- by 6-Foot Supersonic Wind Tunnel at Mach Numbers from 1.49 to 1.98. II - Presentation and Analysis of Force Measurements. NACA RM E50D28, 1950.

4. Stanton, T. E.: On the Effect of Air Compression on Drag and Pressure Distribution in Cylinders of Infinite Aspect Ratio. R. & M. No. 1210, British A.R.C., Nov. 1928.

5. Allen, H. Julian: Pressure Distribution and Some Effects of Viscosity on Slender Inclined Bodies of Revolution. NACA TN 2044, 1950.

6. Rae, R. S., and Ward, G. N.: The Effect of Boundary Layer on the Wave Lift and Drag of Slender Pointed Bodies of Revolution at Supersonic Speeds. Dept. of Sci. Res. and Experiment, Admiralty S.R.E./Airflow/22, May 4, 1945.

7. Tucker, Maurice: Approximate Turbulent Boundary-Layer Development in Plane Compressible Flow along Thermally Insulated Surfaces with Application to Supersonic-Tunnel Contour Correction. NACA TN 2045, 1950.

8. Tsien, Hsue-Shen: Supersonic Flow over an Inclined Body of Revolution. Jour. Aero. Sci., vol. 5, no. 12, Oct. 1938, pp. 480-483.

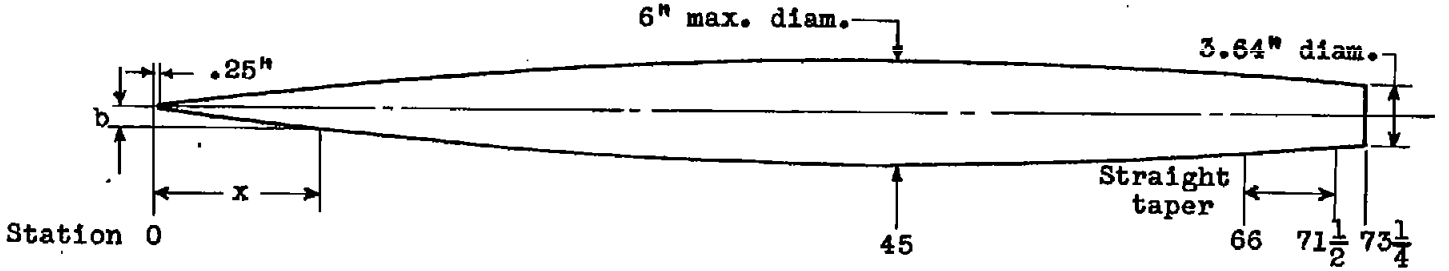

(a) NACA RM-10 half-scale model.

Body defined by equations:

$$b = \sqrt{\frac{c}{2}}\, x\left[2 - \frac{x}{45}\right]$$

$$0 \leq x \leq 73.25$$

$$c = \frac{2}{15^2}$$

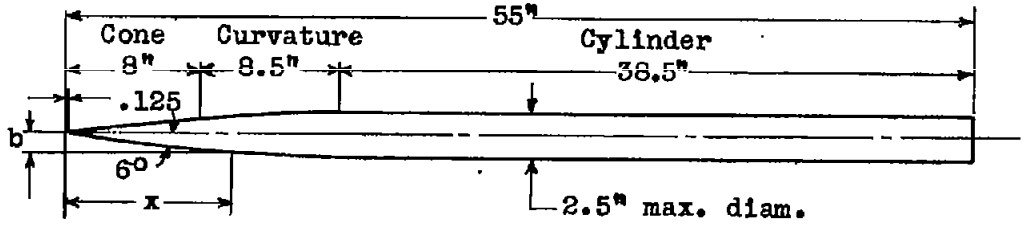

(b) Cone-cylinder model.

Model coordinates for curved section (in.)

x	b
9.000	0.937
10.000	1.020
11.000	1.089
12.000	1.144
13.000	1.187
14.000	1.219
15.000	1.239
15.500	1.245
16.000	1.248
16.500	1.250

Figure 1. - Schematic diagram of NACA RM-10 half-scale model and cone-cylinder model.

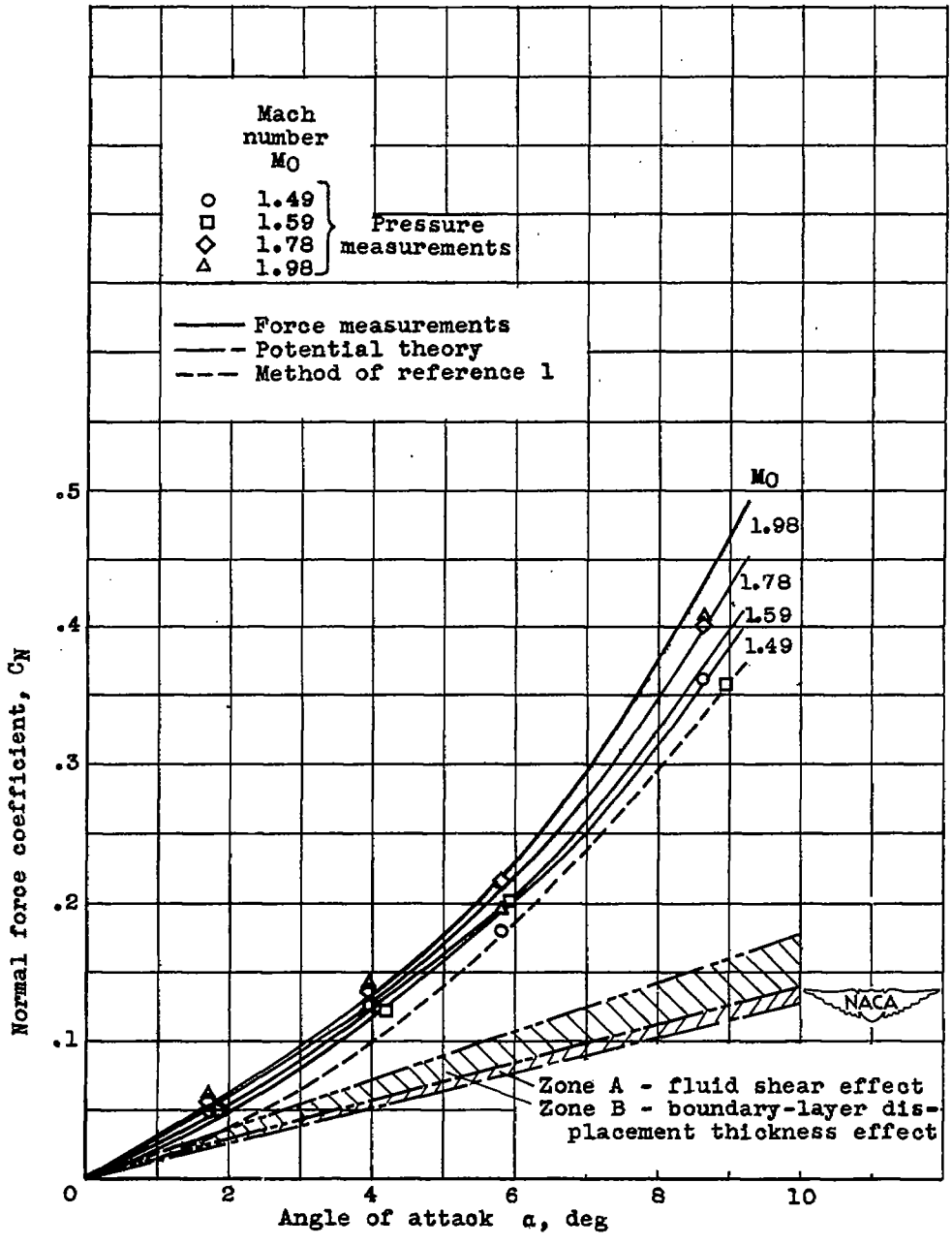

Figure 2. - Experimental and theoretical variation of normal force coefficient with angle of attack at four Mach numbers. RM-10 model.

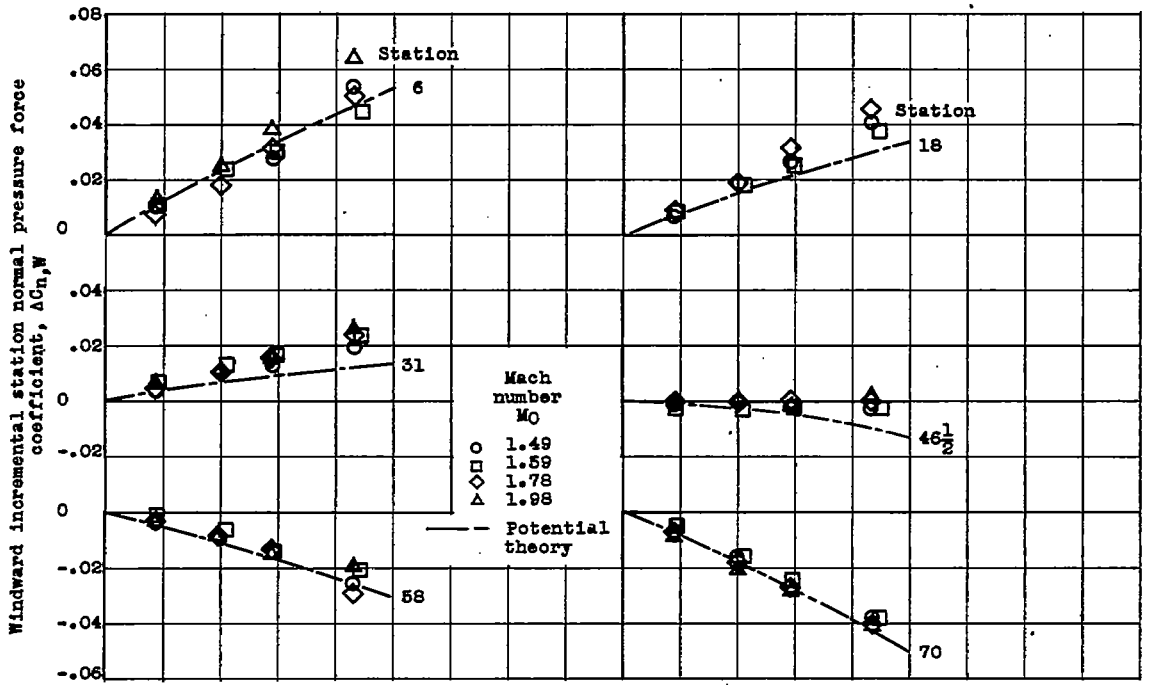

(a) Windward surface.

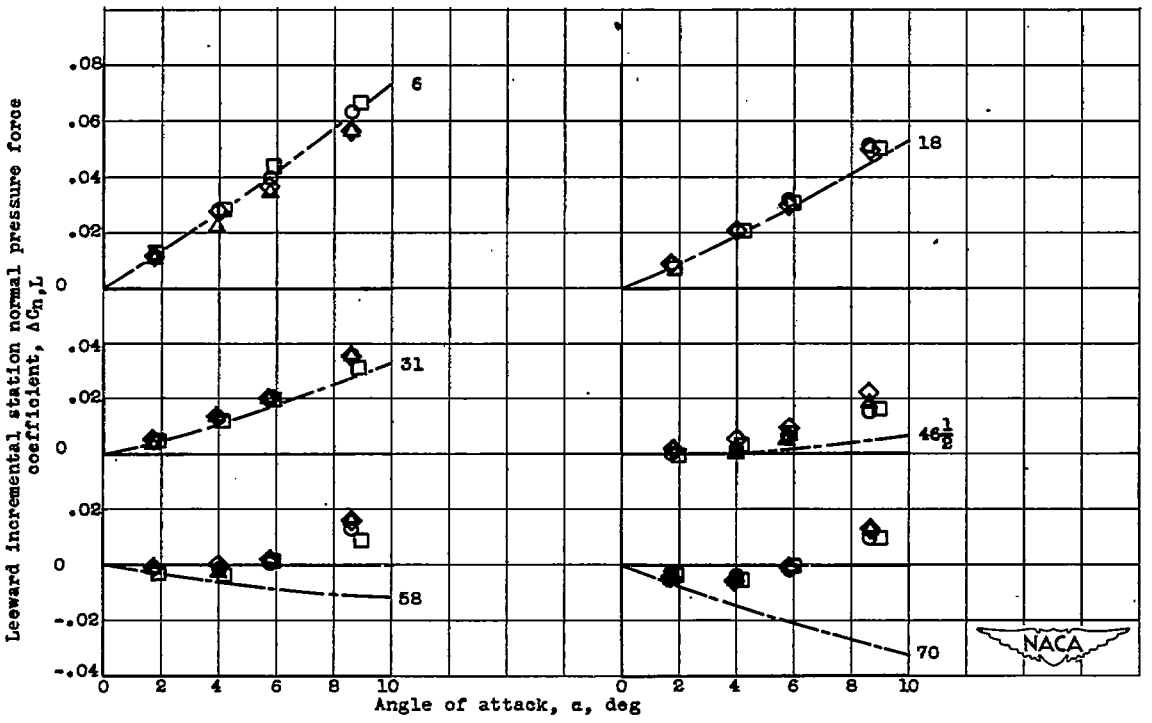

(b) Leeward surface.

Figure 3. - Experimental and theoretical variation of windward and leeward incremental station normal pressure force coefficient distribution with angle of attack for four Mach numbers. RM-10 model.

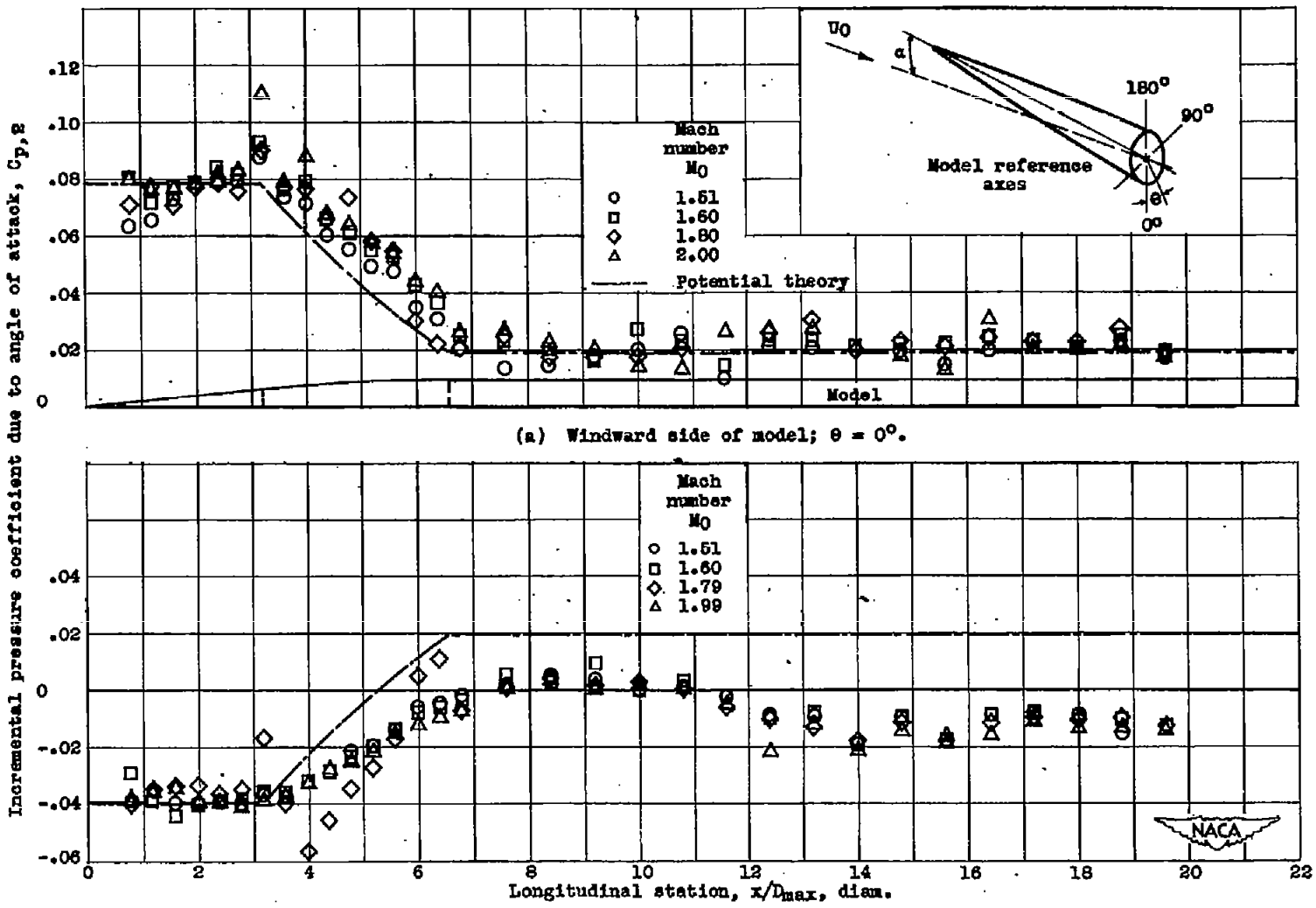

Figure 4. - Experimental and theoretical longitudinal variation of incremental pressure coefficient due to angle of attack for angle of attack of 8° and four Mach numbers. Cone-cylinder model; θ = 0° and 180°.

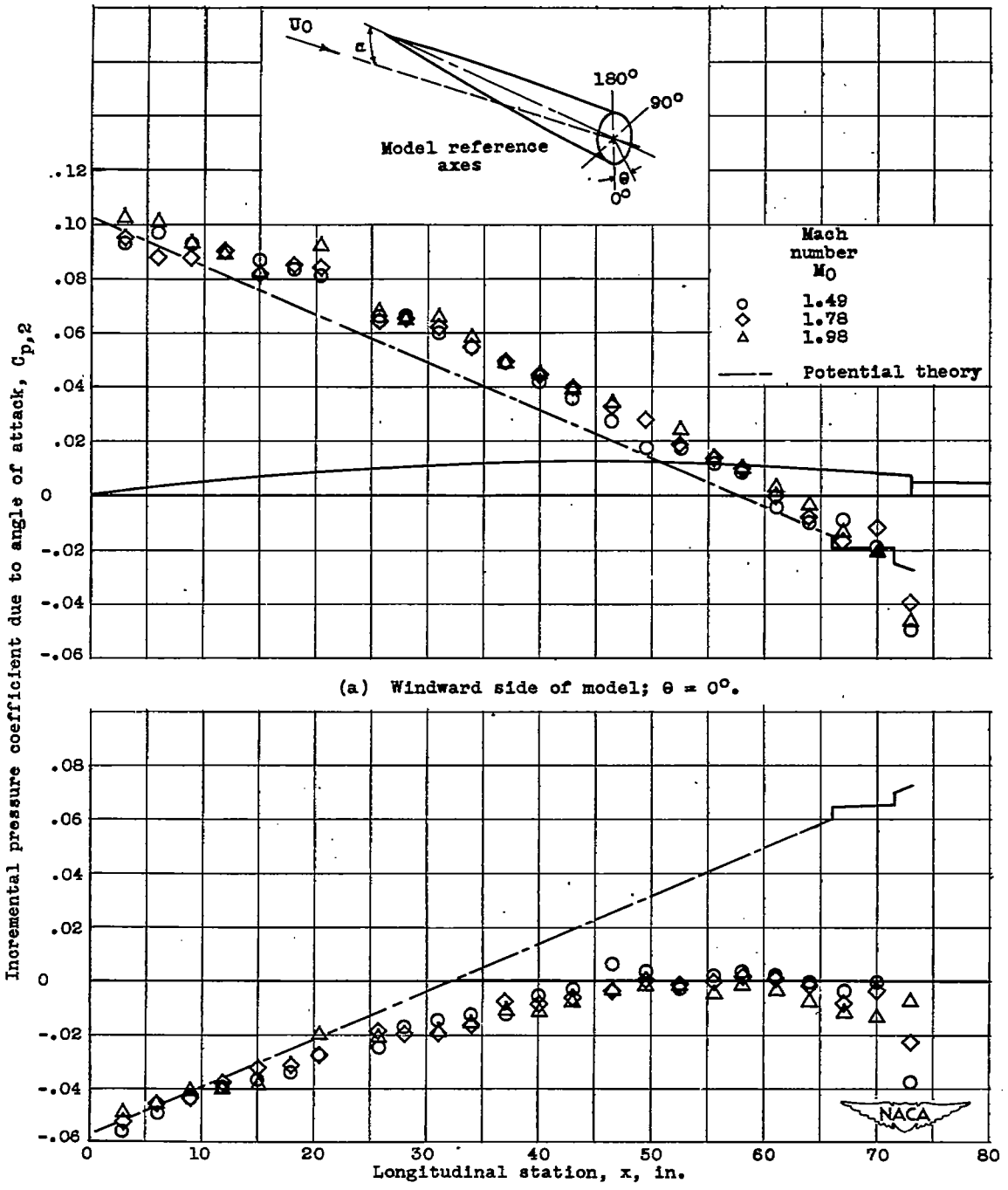

(a) Windward side of model; θ = 0°.

(b) Leeward side of model; θ = 180°..

Figure 5. - Experimental and theoretical longitudinal variation of incremental pressure coefficient due to angle of attack for angle of attack of 8.61° and three Mach numbers. RM-10 model.

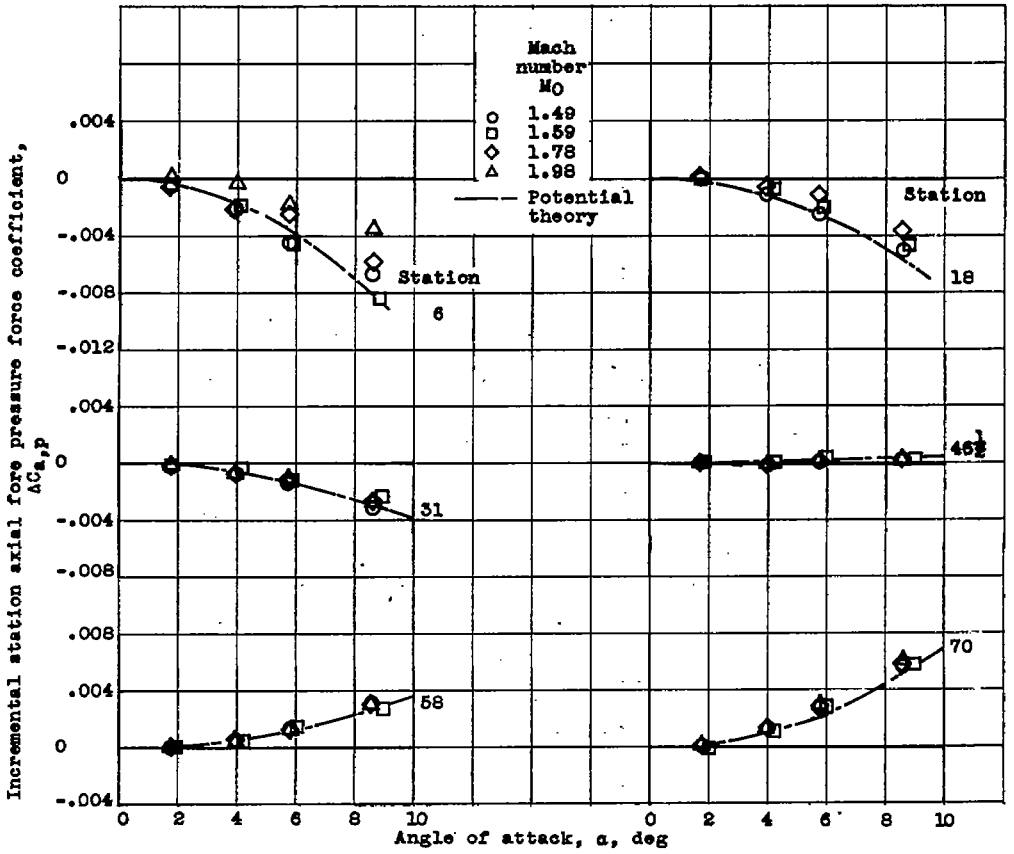

Figure 6. - Experimental and theoretical variation of incremental station axial fore pressure force coefficient distribution with angle of attack for four Mach numbers. RM-10 model.

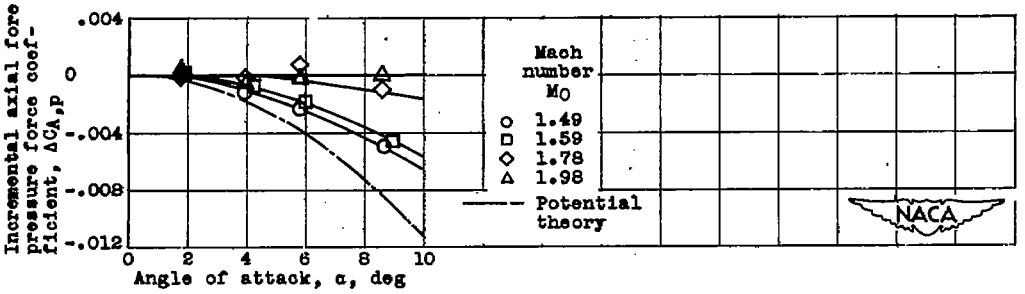

Figure 7. - Experimental and theoretical variation of incremental axial fore pressure force coefficient with angle of attack for four Mach numbers. RM-10 model.

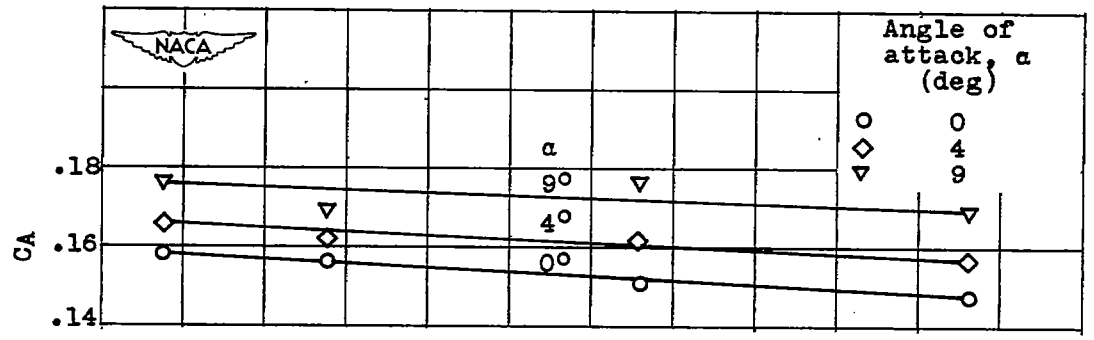

(a) Total axial force coefficient.

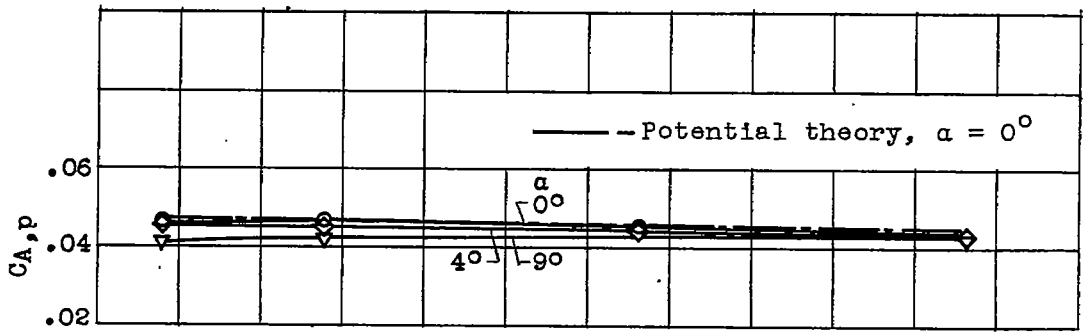

(b) Axial fore pressure force coefficient.

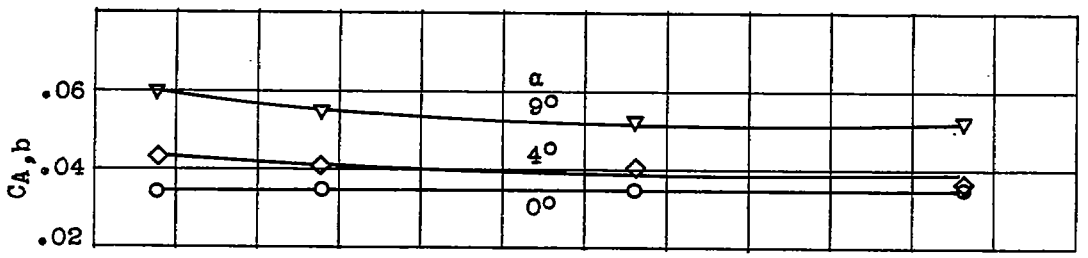

(c) Axial base pressure force coefficient.

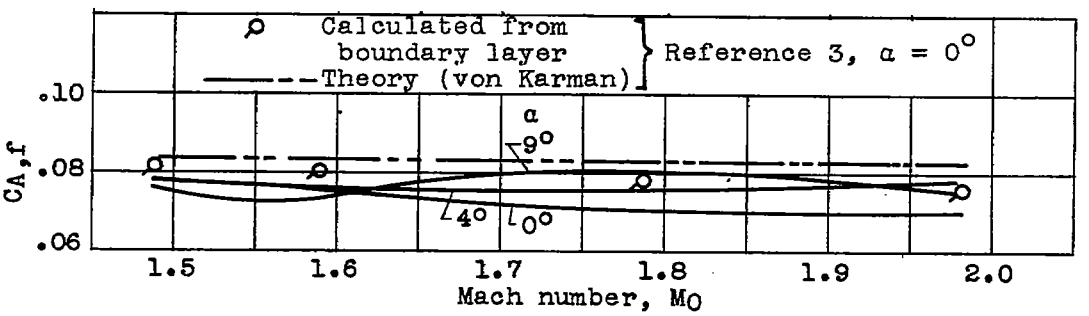

(d) Axial skin friction force coefficient.

Figure 8. - Variation of total and components of axial force coefficient with Mach number for angles of attack of 0°, 4°, and 9°. RM-10 model.

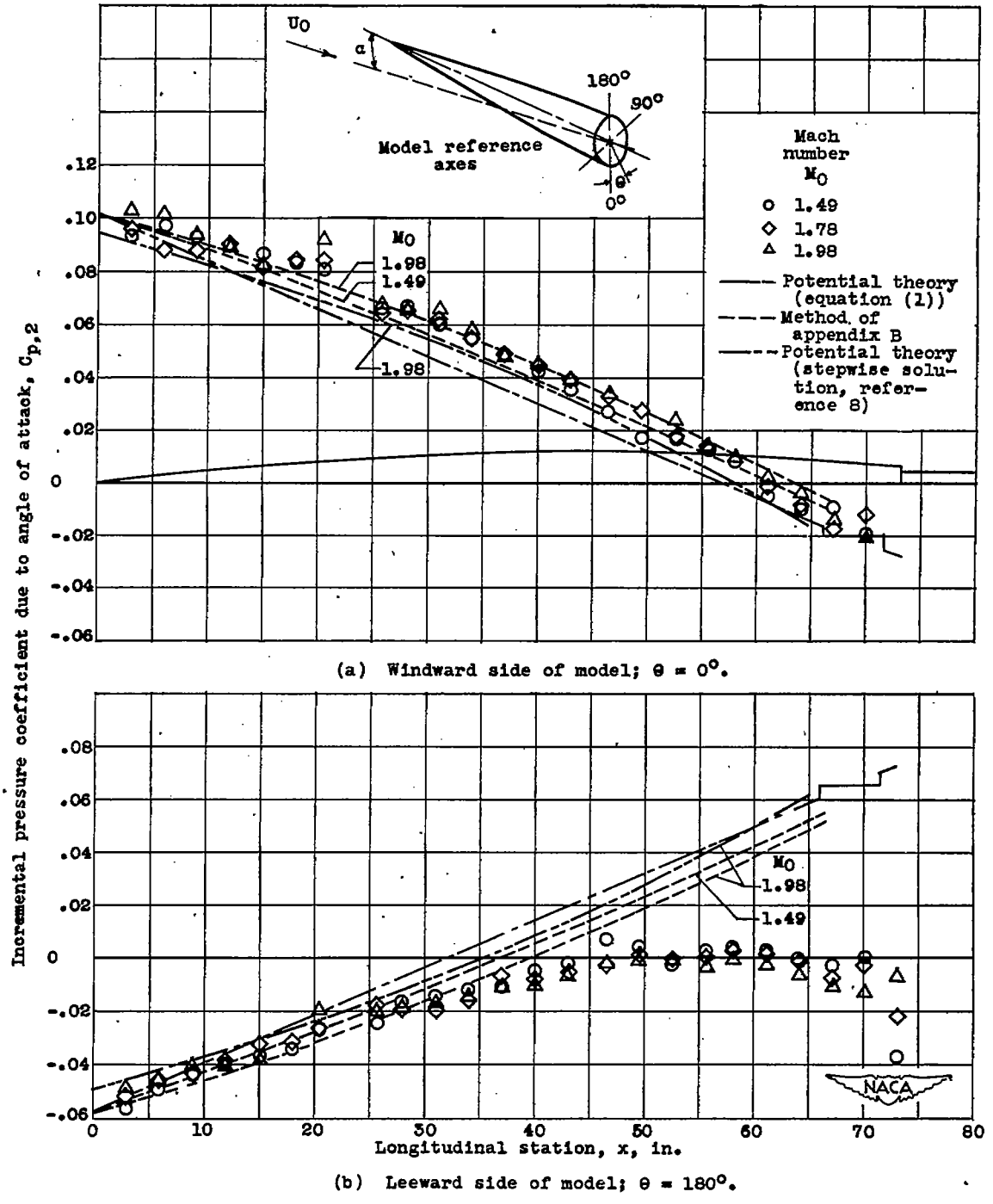

Figure 9. - Experimental and theoretical longitudinal variation of incremental pressure coefficient due to angle of attack for angle of attack of 8.61° and three Mach numbers. RM-10 model.

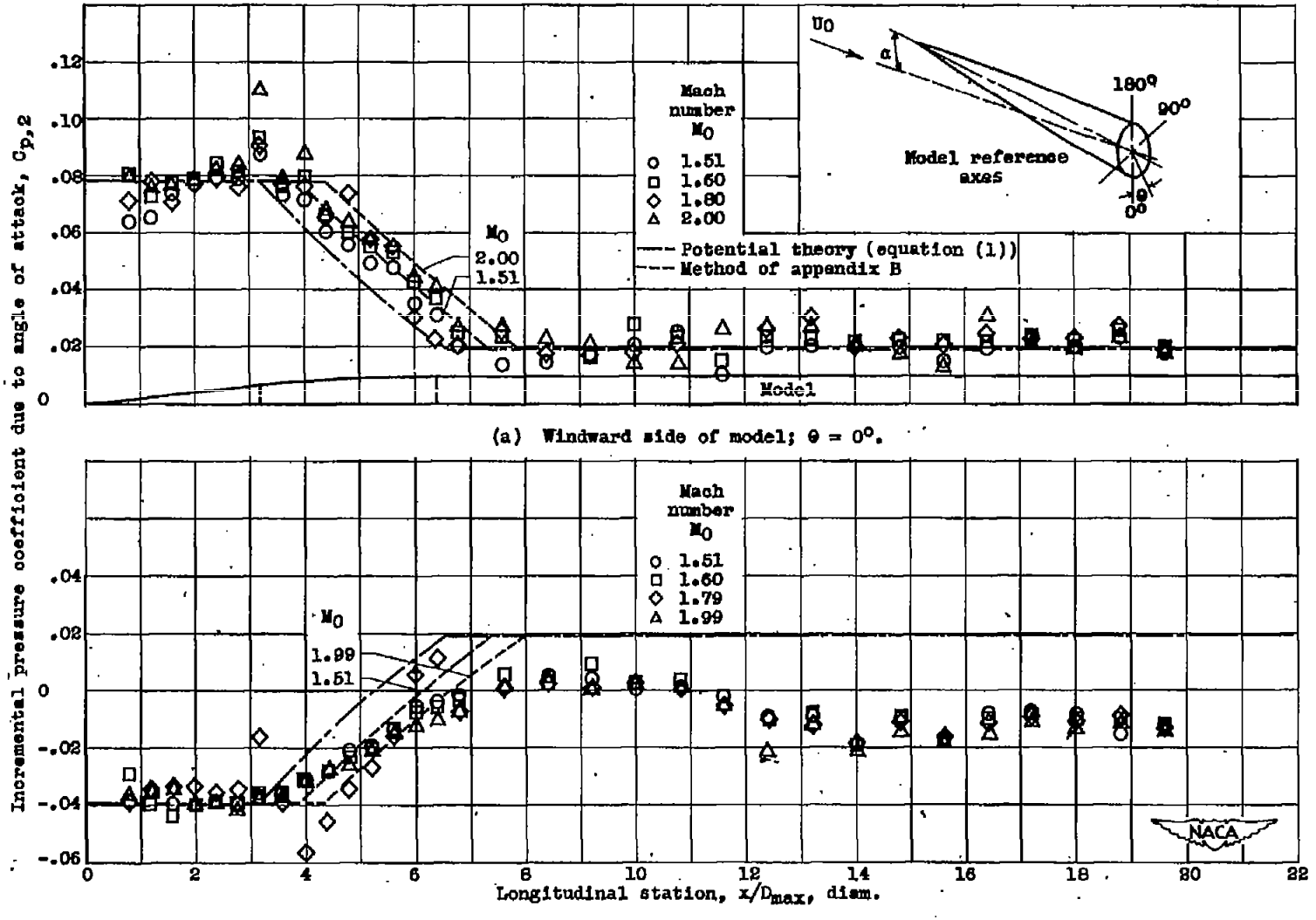

Figure 10. - Experimental and theoretical longitudinal variation of incremental pressure coefficient due to angle of attack for angle of attack of 8° and four Mach numbers. Cone-cylinder model; θ = 0° and 180°.

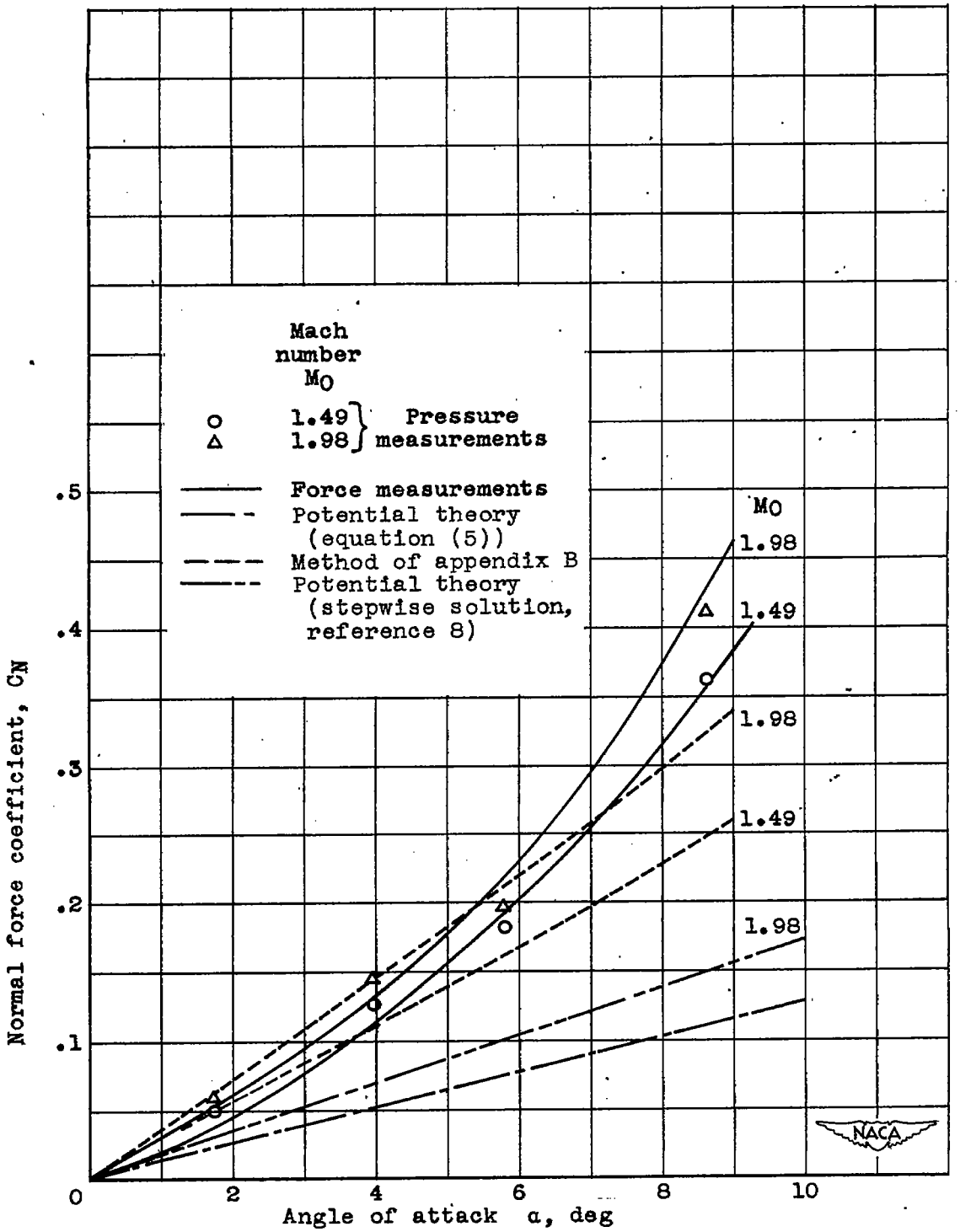

Figure 11. - Comparison of modified theory with experimental normal force coefficient at angle of attack. RM-10 model.

NACA-Langley - 12-12-50 - 525